

Formation of anionic C, N -bearing chains in the Interstellar medium via reactions of H^- with HC_xN for odd-valued x from 1 to 7

F. A. Gianturco¹, M. Satta², E. Yurtsever³, R. Wester¹

Francesco.Gianturco@uibk.ac.at

Received _____; accepted _____

¹Institut für Ionenphysik und Angewandte Physik Universität Innsbruck, Technikerstr. 25/3, A-6020 Innsbruck, Austria

²CNR-ISMN and Dept of Chemistry, The University of Rome Sapienza, P.le A. Moro 5, 00185 Rome, Italy

³Dept of Chemistry, Koç University, Rumelifeneriyolu, Sariyer, TR-34450, Istanbul, Turkey

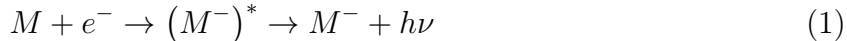
Abstract

We investigate the relative efficiencies of low-temperature chemical reactions in the Interstellar medium (ISM) with H^- anion reacting in the gas phase with cyanopolyne neutral molecules, leading to the formation of anionic C_xN^- linear chains of different length and of H_2 . All the reactions turn out to be without barriers, highly exothermic reactions which provide a chemical route to the formation of anionic chains of the same length. Some of the anions have been observed in the dark molecular clouds and in the diffuse interstellar envelopes. Quantum calculations are carried for the corresponding reactive potential energy surfaces (RPESs) for all the odd-numbered members of the series ($x=1, 3, 5, 7$). We employ the Minimum Energy paths (MEPs) to obtain the relevant Transition State (TS) configurations and use the latter within the Variational Transition State (VTS) model to obtain the chemical rates. The present results indicate that, at typical temperatures around 100 K, a set of significantly larger rate values exists for $x=3$ and $x=5$, while are smaller for CN^- and C_7N^- . At those temperatures, however, all the rates turn out to be larger than the estimates in the current literature for the Radiative Electron Attachment (REA) rates, thus indicating the greater importance of the present chemical path with respect to REA processes at those temperatures. The physical reasons for our findings are discussed in detail and linked with the existing observational findings.

Keywords: astrochemistry, ISM: clouds, molecular processes

1. Introduction

The possibility of having molecular systems formed as stable species with a negative charge (anionic molecules) and to have them exist in detectable amounts in the Interstellar Medium (ISM), more specifically in cold dark clouds environments, was put forward several years ago by various authors (Dalgarno 1973; Sarre 1980; Herbst 1981; Herbst and Woon 1997)). They further suggested that carbon chains and hydrocarbon radicals would have large and positive electron affinities (EA) and could therefore be more likely to lead to anion formations via the energy-releasing mechanism of Radiative Electron Attachment (REA). The latter process would occur from the interactions of such molecules with the free electrons generated in the diffuse regions by H, He photoionization. The recombination process would then be:

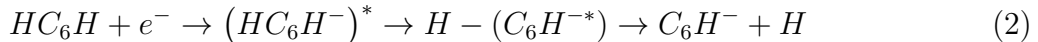


They further surmised that the above processes would provide efficient mechanisms for stabilizing molecular anions when the initial neutrals were made up of more than four or five atoms (Herbst and Osamura 2009)). The experimental, astrochemical evidence for the presence of such species was only provided later on, when an unidentified series of lines were detected in a radio astronomical survey of the evolved carbon star IRC+10216 by Kawaguchi et al. (Kawaguchi et al. 1995), and was conclusively assigned to the spectrum of C_6H^- by Mc.Carthy et al. (McCarthy et al. 2006)) on the basis of laboratory rotational spectroscopy and separate observations toward the Taurus Molecular Clouds 1 (TMC-1(CP)). Additional anionic molecules were observed later on by (Cernicharo et al. 2007) (C_4H^-), by (Remijan et al. 2007) (C_8H^-) and by (Thaddeus et al. 2008) (C_3N^-) in the envelope of IRC+10216 . In the TMC-1 the C_8H^- anions was additionally observed by (Brunken et al. 2007), the largest anionic molecular chain observed thus far. Additional observations on molecular

negative ions were surveyed by (Gupta et al. 2007) who observed C_6H^- in two further sources: the pre-stellar cloud L1544 and the protostellar object L1521F.

Since polyatomic molecules with a negative charge have turned out to be present under different conditions and in significant quantities (e.g., the measured column density of C_6H^- in the TMC-1(CP) was found by (Mc Carthy et al. 2006) to be 10^{11} cm^{-2}), it is reasonable to expect that they also play a significant role in the chemistry of the dark molecular clouds and at the low temperatures assigned to these regions. Hence, it becomes relevant to investigate in more detail additional possible formation paths of such stable anionic species by chemical routes.

From the theoretical and computational standpoints we have already studied in recent years, although on different molecular partners, the general dynamics which could be driven by the free electrons available in that environment and the important role played by intermediate, metastable anions as molecular gateways to the final, anionic species which are experimentally detected. For example, the resonant attachment of slow electrons to $NCCN$ has been studied a while ago in our group (Sebastianelli and Gianturco 2010), while we have also analysed the possible fragmentation decays of HC_3N and HC_5N upon electron attachment (Sebastianelli and Gianturco 2012), as well as carrying out a detailed study of resonant electron attachment to HC_4H (Baccarelli et al. 2013). A more extensive analysis on the dynamics of electron attachment to non-polar hydrocarbon chains like HC_nH (with n from 4 to 12) at the expected low-energies of planetary atmospheres and dark molecular clouds, was also carried out by us (Carelli et al. 2013). In that work it was specifically shown that the attachment mechanism is driven by the prior formation of metastable anions from asymmetrically deformed non-polar polyynes, giving rise to complex intermediates of polar radical anions plus H-atom stretched configurations:



where the intermediate system can initially form its closed-shell anion as a dipole-bound state (DBS) partner. The latter can then decay into the more stable anionic valence-bound states (VBS), after internal-energy redistribution and ejection of one terminal hydrogen atom. The above chain of events is reminiscent of the indirect REA mechanism (IREA) introduced more recently by (Douguet et al. 2013), where the dissipation paths of the large amount of energy which has to be released upon electron attachment in systems with large and positive EA values was suggested to occur via an electron-vibration nonadiabatic coupling mechanism. They have shown however that this IREA mechanism, and indeed also the REA mechanism of eq. (1), is unfortunately rather inefficient for the smaller radical chains like C_2H^- and C_4H^- , thereby calling into question the relevance of such pathways for the formation of observable quantities of the anions of the present molecules. It is therefore important to further explore and understand which other mechanisms could be responsible for the formation of the smaller (C, N)-chains anions under ISM conditions.

To extend the chemical formation option, we wish to explore in the present study a "chemical" stabilization of the anions which involve four of the members of the C -bearing linear chains that terminate with the cyano group (Morisawa et al. 2005)). We shall therefore look at the efficiency of the formation of such anions by examining the reaction of H^- with non-polar precursors of the cyanopolyne series, the (HC_xN) molecules, in the gas-phase :



where the length of the odd-numbered chains goes in our study from $x = 1$ to $x = 7$.

The importance of H^- as a chemical partner has been suggested before, given its likely existence through cosmic rays which act during ion-pair reactions within the inner cores (radius $\leq 10^6 AU$) of the prestellar envelopes (Prasad and Huntress 1980)), although little is known so far on the details of its actual mechanism under the above conditions (Mackay et al. 1977)).

Therefore, if the presence of H^- could be in sufficient amounts to provide a useful chemical partner, then we shall show that the above reaction is indeed an interesting alternative. They are in fact, as discussed below, markedly exothermic processes where the final product formations involve an electron transfer (ET) mechanism accompanied by the formation of a new H_2 bond into a separate molecular product from the final anion.

In an earlier study on the smaller members of the cyano derivatives, CN^- and C_3N^- (Satta et al. 2015) we have indicated that the chemical nature of their reactions with H^- , i.e. the suggested mechanism of an ET process occurring along with the energy release from the H_2 formation, makes the production of their anions to be exothermic and to occur without an intermediate energy barrier between reactants and products, although a configurational Transition State (TS) is observed. It thus becomes interesting to computationally extend the study of these reactions to verify their behaviour for larger members of the series, as well as revisiting the earlier results by using an improved description of the quantum chemical interaction forces.

In the following sections we shall investigate this point for the reactions involving the first four members of the cyanopolyne series. The next Section 3 analyses the overall shapes of the various RPESs, while Section 4 calculates the corresponding reaction rates over a range of temperatures representing the colder dark cloud conditions and the warmer circumstellar envelopes which are of interest in our study. Section 5 will give our present conclusions and also link them with the existing observational studies on the abundances of

the cyanopolyynes anions.

2. Quantum chemical calculations

Before starting our analysis of the dynamical features of the reactive partners in eq. (3) we need to look into the quantum structural properties that we have obtained for all partners in the considered processes. All the ab initio structural calculations were carried out using the MOLPRO suite of codes (Werner 2006)), unless otherwise stated. In order to better analyse visible trends along the present series of linear anions, we have repeated the calculations for the smaller terms of the series, the $x = 1$ and the $x = 3$ molecular anions already investigated before (Satta et al. 2015)). We have also extended the analysis of the kinetics of CN^- formation by considering both isomeric structures of the initial molecule, HCN and HNC . More details on this aspect of the discussion will be given below.

The method employed here has been the Coupled-Cluster-Single-Double-Perturbative-Triple-Excitation (CCSD(T)) and the quality of the chosen basis sets is defined as augmented-correlation-consistent, corrected up to triple-zeta expansions : aug-cc-p-VTZ . All the present acronyms are explained in detail in the MOLPRO suite of codes (Werner 2006)). All the molecular reagents, as already known, turned out to be linear in the most stable ground electronic states which correspond to closed-shell structures. Their optimized geometries are presented in Table 1. We also report in that Table the geometries of the isomer radicals C_xNH so that they can be compared with the corresponding structures of the HC_xN species.

C_xN^-	x=1	x=3	x=5	x=7
C1C2	—	1.263	1.271	1.275
C2C3	—	1.364	1.342	1.333
C3C4	—	—	1.246	1.255
C4C5	—	—	1.352	1.329
C5C6	—	—	—	1.247
C6C7	—	—	—	1.351
C(last)N	1.191	1.187	1.188	1.188
HC_xN	x=1	x=3	x=5	x=7
C1C2	—	1.217	1.222	1.224
C2C3	—	1.372	1.359	1.354
C3C4	—	—	1.228	1.235
C4C5	—	—	1.364	1.347
C5C6	—	—	—	1.233
C6C7	—	—	—	1.361
C(last)N	1.167	1.177	1.180	1.181
C1H	1.065	1.063	1.064	1.063
C_xNH	x=1	x=3	x=5	x=7
C1C2	—	1.274	1.284	1.289
C2C3	—	1.313	1.305	1.303
C3C4	—	—	1.263	1.271
C4C5	—	—	1.300	1.292
C5C6	—	—	—	1.269
C6C7	—	—	—	1.298
C(last)N	1.177	1.178	1.184	1.187
NH	0.998	0.995	0.996	0.996

Table 1: Computed, optimized geometries for the neutral radicals and negative $^1\Sigma$ molecules of present study. All species are linear and the distances are in Å

One clearly sees from the Table’s data that only minor differences in the geometries occur when going from the HC_xN to C_xHN : we shall further analyse below the possible effects on the energy changes of these exoergic reactions. The total energies for the ground states of reagents and products are reported in Table 2

Molecule	aug-cc-pVTZ energy
H_2	-1.172613
H^-	-0.526562
C_3N^-	-168.723503
C_5N^-	-244.743867
C_7N^-	-320.762897
HC_3N	-169.288765
HC_7N	-245.302425
HC_7N	-321.317307

Table 2: Computed ground state total energies for reactants, using the CCSD(T) method described in the main text. All values are in units of hartrees.

As mentioned earlier, all the present reactions are exothermic processes involving polar targets. To check on the quality of our description of them, we report in Table 3 the calculated values of the permanent dipoles of the molecular partners undergoing the electron transfer (ET) process during the reactions.

CN	RODFT(B3LYP)	ROMP2	ROCCSD(T)	Anion*
6-311G(2df,2pd)	-1.3058	-2.2765	-2.2569	0.69
6-311++G(3df,3pd)	-1.3811	-2.3256	-2.3087	
cc-pVTZ	-1.3222	-2.2847	-2.2672	
aug-cc-pVTZ	-1.3794	-2.3233	-2.3069	

C_3N	—	—	—	Anion*
6-311G(2df,2pd)	-2.8394	-3.1759	-3.1753	2.72
6-311++G(3df,3pd)	-2.9571	-3.2539	-3.2533	
cc-pVTZ	-2.8807	-3.2058	-3.2052	
aug-cc-pVTZ	-2.9552	-3.3252	-3.2506	
cc-pVQZ	-2.9340			
aug-cc-pVQZ	-2.9554			

C_5N	—	—	—	Anion*
6-311G(2df,2pd)	1.2490	-0.3117		5.61
6-311++G(3df,3pd)	1.2796	-0.3310		
cc-pVTZ	1.2997	-0.2992		
aug-cc-pVTZ	1.2932	-0.3181		

C_7N	—	—	—	Anion*
6-311G(2df,2pd)	0.7796	-0.4389	-0.4389	4.19
6-311++G(3df,3pd)	0.7888	-0.4648		
cc-pVTZ	0.8083	-0.4352	-0.4352	
aug-cc-pVTZ	0.7978	-0.4541		

Table 3: Computed permanent dipole moments (in units of Debye) for the neutral counterparts of the final product. RODFT, ROMP2 and ROCCSD(T) denote restricted-open-shell calculations. *Anion values are from Carelli et al. (2014)

It is interesting to note that the dipole moment of the CN radical is found, ensuing the largest basis set in the bottom line in the Table, to vary between -1.379 and the CCSD(T) approach (last column to the right) of -2.307 Debye. The experimental value of a while ago is 1.45 Thomson and Dalby (1968) while a recent calculation Fortenberry and Crawford (2011) yielded a value of -1.47.

For the C_3N , C_5N and C_7N the largest basis set was used within the Density Functional approach (DFT) using the B3LYP exchange functional model, providing decreasing values of -2.95, +0.80 and +1.30 Debye in Table 3. Our earlier calculations had yielded values of -3.0, +0.80 and 1.29: no experimental values or earlier calculations exist on the radicals, as discussed by Carelli et al. (2014). On the other hand, all the corresponding anions have very different dipole moment values, as reported in the last columns of table 3 and as computed earlier by Carelli et al. (2014): no experimental values are available for the closed-shell anions, while earlier calculations by Botschwina and Oswald (2008) and by Kolos et al. (2008) yielded dipole moment values with the same orientation (i.e. along the z-axis and now pointing from the N to the C atoms in each member of the series) and about 20% larger.

In all cases, therefore, the dipole moment values increase dramatically in going from the radical to the closed-shell anionic structures. Along the same series of cyanopolynes the corresponding electron-affinities (EA) also increase rather markedly from the n=1 member (+3.8 eV) to the n=7 member (+4.61 eV) as discussed already in our earlier study Carelli et al. (2014). This means that the occurrence of the ET step during the reactions we are going to discuss affords large energy releases when the electron moves from the H^- partner (with an EA value of 0.754 eV Shiell et al. (2000)) to the N-end of the final linear chains with much larger EA values. This aspect will be further discussed below in more detail.

We have computed again the EA values at the equilibrium geometries of the present

radicals and found the results reported below in Table 4.

	Present Calculations	Expt(Carelli et al. (2014))	Calculations(Carelli et al. (2014))
CN	4.00	3.86	3.80
C_3N	4.64	4.59	4.40
C_5N	5.09		4.59
C_7N	5.51		4.61

Table 4: Computed EA values at the CCSD(T) level of calculation of the present study (eV)

We can see from the Table that all the present radicals have very large EA values, thus making the ET process from the H^- reagent into the final anions a strongly exothermic process leading to the TS formation complex before the additional energy release due to the formation of the neutral H_2 bond during formation of the final molecular products. We shall further illustrate below in more detail the energetics of the present reactions.

If we look at the data at the CCSD(T) level of calculations, we see that all the reactions involving the HC_xN reagents are consistently exothermic along the series, varying by more than 10% as x increases from 1 to 7: as we shall further see below, none of them shows any barrier from reagents to products, thus confirming their feasibility at the low temperatures of the DMC environments.

Additionally, we see that the same set of reactions involving their isotopologue variants, occurs with the HNC_x series of reagents (lower panel in Table 5).

$H^- + HC_xN \rightarrow H_2 + C_xN^-$			
x	MP2	MP2+ZPE	CCSD(T)
1	2.11	2.14	2.12
3	2.17	2.19	2.20
5	2.37	2.40	2.38
7	2.53	2.58	2.49
$H^- + HNC_x \rightarrow H_2 + NC_x^-$			
x	MP2	MP2+ZPE	CCSD(T)
1	2.89	2.90	2.76
3	4.59	4.56	4.48
5	5.19	5.17	5.14
7	5.54	5.55	

Table 5: Computed exothermicity values for the two series of reactions involving both isotopologue forms. Units are in eV

The exothermicity values increase quite markedly: an increase of about 0.64 eV for the HCN/HNC case, to more than 2.60 eV for the HNC_7 case. This is an interesting result for which, however, we have little observational information for the members with x from 3 to 7. On the other hand, the HCN/HNC isotopologues have been extensively observed in many astrophysical environments: from diffuse and translucent interstellar clouds in Listz and Lucas (2001); Turner et al. (1997), to dense interstellar clouds: see Mily-Blant et al. (2010), to star-forming regions in jin et al. (2015), to protoplanetary disks: Graninger et al. (2015), to external galaxies as in Gao and Solomon (2004) as well as in comets: Lis et al. (2008) and planetary atmospheres: Moreno et al. (2011).

Likewise, the HCN/HNC abundance ratios have also shown marked changes between

different astrochemical environments. In the dense interstellar clouds, in fact, the gas is shielded from external UV starlight and the abundance ratio was found to be around 1.0 in Sarrasin et al. (2010). On the other hand, in regions exposed to UV photons HCN was found to be more abundant than HNC by a factor of 5 in both diffuse clouds: Listz and Lucas (2001) and in PDR environments as in Hogerheijde et al. (1995). It therefore stands to reason that both reactions could occur with H^- , thereby increasing the probability of forming CN^- , as we shall further discuss below.

Although, for the longer members of the series, we know little about the ISM relative abundances of their isomeric structures, our findings provide already a relevant result in the sense that, within the chemical route that we intend to explore in the present study, our data from Table 5 indicate that both isomers would be important to investigate in order to consider both chemical paths to the formation of their corresponding anions. However, we shall mainly discuss in the following the reactions with the HCN and HNC reagents, to show these paths to forming CN^- as being equally possible in the different environments of the ISM we are analyzing.

3. The shapes of the reactive surfaces

As discussed before, all reactions of interest in this study are strongly exothermic. Furthermore, our previous experience with such process, as discussed in Gianturco et al. (2016); Satta et al. (2015), has shown us that they are dominated by a collinear Minimum Energy Path (MEP) and without any barrier existing between reagents and products. The suggested mechanism, in fact, is given in Gianturco et al. (2016); Satta et al. (2015) as one in which the initial ET process occurs during the approach between the two hydrogen atoms: the H-C bond is stretched as the H anion is approaching, thereby allowing for the starting of the electron transfer exothermic step from the approaching H^- initially to the C-end

of the molecular partner but finally, and chiefly, to the N-end of the radicals (C_xN^-). The formation of a TS configuration as the partners approach each other more closely now further leads to additional energy release into the final products by forming a neutral, vibrationally cold H_2 molecule that separates from the highly stretched configuration it has within the transition complex. A pictorial representation of the 3D surface describing the reaction (RPES) is reported by Figure 1, where the two panels compare the two isomeric variants we have discussed before. The left panel therefore shows the reaction of H^- with HCN, while the one on the right reports the same reaction but with HNC: both sets of reagents yield H_2 and CN^- as products.

It is evident from a perusal of both surfaces that the two reactions proceed in the same fashion: no energy barriers between reagents (on the left region of each RPES) and products (on the right region of the same surfaces) and a marked exothermicity which, for the case of the HNC, is even larger by more than 0.5 eV (see data in table 5). We therefore expect that both reactions can play a role in the ISM regions where both molecules in question have been observed

It is also interesting to note here that both energy surfaces show an intermediate, smaller energy minimum at the stretched distances of the $C - H$ end of the partner molecular chain (around 2 to 4 Å) and at even larger values of the $H - H$ distances of about 4 Å. One could suggest that in that outer well region the initial ET step begins to occur while the molecular hydrogen is still strongly vibrationally excited and the terminal H atom has moved far away from the residual cyano derivative.. In other words the excess electron would initially "transfer" to the H-end of the chain and finally to the CN-end of the new anion after the H_2 is formed as one of the molecular products. It is thus at the second energy minimum, which is now deeper and occurs at shorter $C - H/N - H$ distances that the neutral, H_2 molecule starts to get formed (second exothermic step) by releasing its

Collinear approach

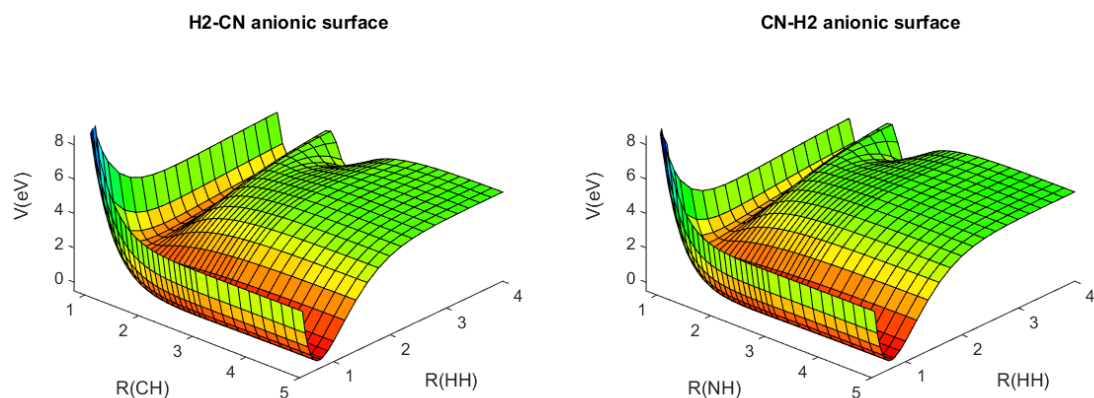


Fig. 1.— Computed Reactive PES for the formation of CN^- from either $\text{H}^- + \text{HCN}$ (left panel) or $\text{H}^- + \text{HNC}$ (right panel). See main text for further discussion.

vibrational energy content and thus reaching the variationally optimized TS which evolves towards finally producing H_2 in its vibrational ground state as it separates from the anionic product.

In the two panels of Fig. 2 we further report the RPES shape for the reaction involving the next member of the cyanopolyynes series: the HC_3N neutral partner of H^- . The upper panel of the Figure shows in the forefront the H^- approach to the HC_3N reagent (from right to left) and the clear exothermic, barrierless path down to H_2 formation and C_3N^-

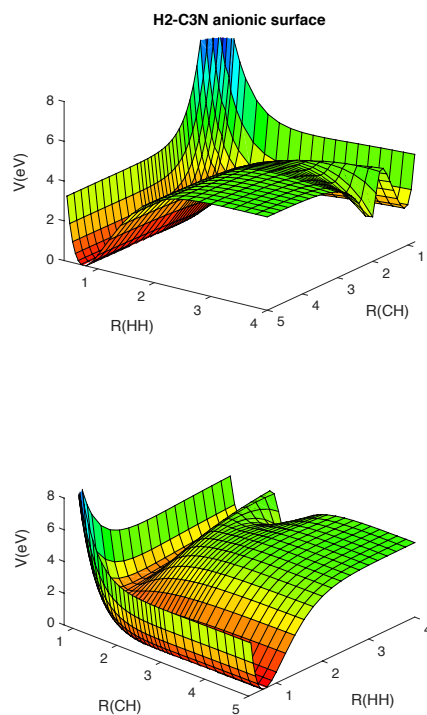


Fig. 2.— Two different views of the reactive PES for the $H^- + HC_3N$ reaction. The upper panel shows the entrance channels on the upper right region of the RPES, while the lower panel reports the products' channel on the lower right portion of the surface. See main text for further details.

separation on the further valley going out on the left of that panel. On the other hand, the rotated view presented in the lower panel indicates on the extreme left the incoming, exothermic path for the H^- approach to the C-H end of HC_3N , followed by the further, exothermic outgoing C_3N^- and of the cold H_2 formation along the valley shown in the forefront, from left to right.

From the upper view of the RPES shown in that Figure we see even more clearly the

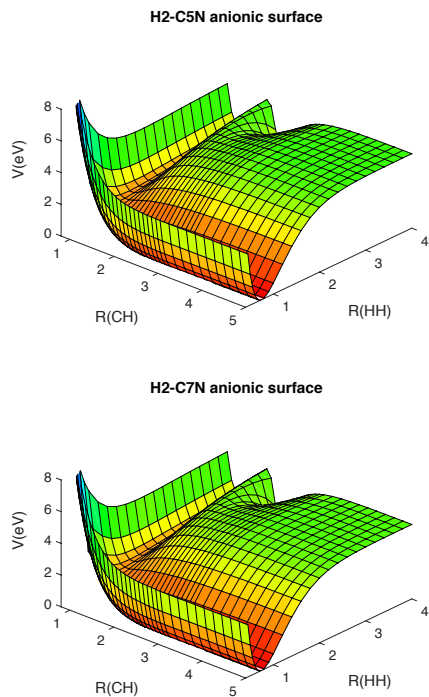


Fig. 3.— Computed 3D presentation for the collinear MEPs relative to the next larger members of the cyanopolyynes series. Upper panel: $H^- + HC_5N$; lower panel: $H^- + HC_7N$. See main text for further details.

role of the outer, shallower energy well that we associate to the initial ET step while the $H - H$ bond is still describing a highly vibrationally excited pair of H atoms, the external one being also far away from the residual cyano derivative fragment. It is thus an indication of the occurrence of a non-adiabatic curve-crossing effect that transfer the H^- charge to the terminal H atom of the cyanopolyynes partner. . It is then the deeper well located at the shorter C-H distances which will permit the exothermic release of that vibrational energy along the evolution of the variationally optimized TS complex (as we shall discuss in more

detail in the next Section) that can now decay into the final "cold" molecular products without any intermediate energy barrier and having completed the ET step to the final anionic product.

In conclusion, this member of the cyanopolyynes series also show its reaction with H^- to be a barrierless, exothermic process along a nearly collinear path. Along that path, in fact, one gains energy by the occurrence of an initial Electron-Transfer (ET) process which takes place for highly stretched $C-H$ and $H-H$ bonds between partners. The release of that vibrational energy in both bonds helps the TS formation at the bottom of the RPES, at the start of the MEP path. As we shall further explain in the next Section, along such reaction path the formation of a cold $H-H$ neutral molecule plus the outgoing anionic linear chain as one of the products can now occur in a strong exothermic and barrierless fashion.

The same general features of this reaction are also observed along the collinear MEP energy evolution reported by Figure 3 for the next two members of the series: C_5N^- and C_7N^- .

In both instances the process remains, as before, strongly exothermic and without any barrier between reagents and products after the occurrence of the initial ET step indicated by the presence in both systems of the outer, shallower energy well for vibrationally excited $C-H$ $H-H$ distances. Once the deeper well of the RPES is reached at shorter distances within the complex, the systems reach configurations where both the above bonds are shorter and close to their equilibrium values. This means that the reactions can now follow the exothermic MEP evolutions without any intermediate barrier, as we have already explained before.

Another interesting way of visualizing the exothermicity of the present reactions is shown by the two panels of Figure 4, where we choose as an example the isomer reactions

involving HCN/HNC partners.

Both panels of that figure present the collinear reaction paths after "cold" H_2 formation has occurred and the initial vibrational energy of that bond has been released: the formed anion now recedes from the complex region. The H-H distance is also that of the optimized complex geometry in both cases (see next Section's discussion). The upper panel clearly shows that in both reactions the formed anions leave the complex along a monotonically decreasing path since the formation of a vibrationally cold, neutral H_2 now affords the systems to undergo a substantial energy release without any intermediate barrier.

We have enlarged in the lower panel of the same figure the energy region where either the H-C or the H-N distances are clearly down into a flat outgoing path. It now shows in both cases the presence of a very shallow well indicating the absolute minimum energy location of the complex configurations before the final release of the two products, as mentioned already when analysing the previous figures. Although the reaction with HNC shows a slightly larger well (-0.11 eV vs -0.09 eV) into their configurations of the reaction complex, both systems can easily make out to products even at the lower temperatures, due to the marked shallowness of such small minimum regions. However, this can energetically happen provided the initial ET step has been allowed to occur along the outer wells shown by Figure 2 and already discussed earlier in this Section .

In the next Section we shall be using the present RPES of the colinear approaches to help us to obtain the corresponding reaction rates over a broad range of temperatures, following the nonlinear, 3D model of the Variational Transition State Theory which we shall discuss below. in greater detail

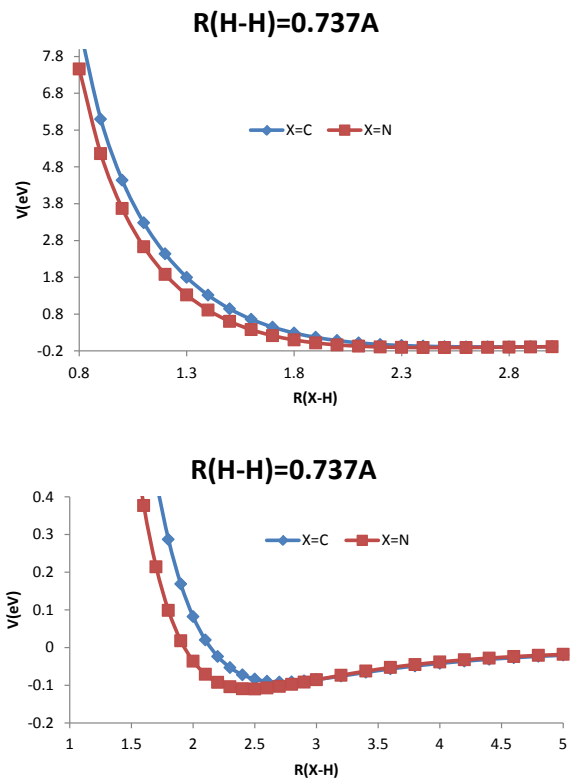


Fig. 4.— Different collinear 'cuts' for the reaction of $H^- + HCN$, given by small lozenges, and $H^- + HNC$, given by large squares, at fixed H-H distances for the geometry of the complex. The 'X' symbols denote the remaining chains from either end of approach for the H^- partner. (colours on line). See main text for further details

4. Modelling the reaction rates

We have seen in the previous discussion that all the reactions evolve on RPESs which are markedly exothermic and present no energy barriers along the MEP evolutions from reagents to products. Furthermore, the calculations of the relative energetics between reagents and products, for all the members of the series we have examined, indicate a marked increase of exothermicity in going from one set of HC_xN partner to the HNC_x

isomeric variants. This last feature will be discussed below, as an example, for the case of HCN/HNC systems.

The special features of the reaction energetics have allowed us to use a version of the RRKM approach based on the Variational Transition State Theory (VTST) treatment for obtaining temperature-dependent rates, as discussed in Fernandez-Ramos et al. (2006) for the case of exothermic, barrierless reactions. This approach is basically assuming that, for the present types of reactions, the formation of a transition-state complex along the exothermic energy path from reactants to products controls the efficiency of product formation via the relative energetics between the partition functions of that complex and those of the final products.

In particular, within the RRKM approach for the description of a TS configuration, one assumes a strong-coupling approximation whereby the degrees of freedom within the TS complex are strongly coupled among themselves and therefore the entire phase-space available will be occupied by the partition functions (PFs) associated to the TS on a shorter time-scale than that of the characteristic reaction time step: see Fernandez-Ramos et al. (2006). This means that, once the TS complex is reached by the reagents along the exothermic MEPs, the reactants are in microcanonical equilibrium. The TS complex partition function, Q_{TS}^\ddagger , can then be obtained as the product of the PFs for the conserved mode partition functions within that complex, Q_{cons}^\ddagger , times the PFs of the translational modes which are evolving along the MEP following the complex geometry, Q_{trans}^\ddagger . The latter modes now make the complex evolve from reagents to products, thereby acting as the active modes of the reaction:

$$Q_{TS}^\ddagger(T) = Q_{cons}^\ddagger(T)Q_{trans}^\ddagger(T) \quad (4)$$

In our case the translational modes for the title reactions will be those indicated

in the 3D energy maps of the previous Section: the $H^- \cdots H$ distance and the $H \cdots C$ distance along the collinear path. We shall see later that such simpler approach holds well for the $x=1$ case, while the larger chains will require a multidimensional optimization along increasingly non-linear TS structures formed along their respective MEPs. The pre-exponential factor of the reaction rate formulations becomes now the only significant part which needs evaluation in order to obtain the required reaction rates $K(T)$. Thus, the latter quantities can now be obtained as the ratios between the relevant PFs of the TS complex and those of the reagents, as a function of the reaction temperatures:

$$K(T) = \frac{k_B T}{h} \frac{Q^\ddagger[H^- - HC_x N]}{Q[HC_x N]Q[H^-]} \quad (5)$$

Here k_B is the Boltzmann constant and h is the Plank's constant. The PFs of the reaction complex are variationally minimized along all the optimized geometries of the MEP. After the variational minimization we therefore obtain at each temperature the TS geometries at the lowest possible energy along the MEP paths and within the VTST model : see Fernandez-Ramos et al. (2006).

It is interesting to note at this point that the rate coefficient as obtained from (5) is mainly controlled, at the lowest temperatures, by the behaviour of the vibrational part of the PF for that specific TS geometry since all other degrees of freedom are now "frozen" to their lowest values. In turn, such low-temperature PFs relate directly to the zero-point energy (ZPE) values of the modes under consideration since Q_{vib} (at low T) can be written as $\propto e^{-E_{ZPE}/KT}$. Thus the overall rates at low-T would be linked with the features of the corresponding ZPE energy values within the PFs:

$$K(lowT) \propto T^2 \exp \frac{-E_{ZPE}^{TS} + E_{ZPE}^{React's}}{k_B T} \propto T^2 \exp \frac{-\Delta_{ZPE}}{k_B T} \quad (6)$$

in the present reactions we have that the $E_{ZPE}^{reacts} = E_{ZPE}^{HC_xN}$ since H^- does not contribute to it. The quantity Δ_{ZPE} thus defines the energy differences between ZPEs of the reactants and those of the TS complex. It therefore controls the slope of the reaction rate $K(\text{lowT})$ which is defined by the above equation: a large value of that difference causes a greater decrease of $K(T)$ as T decreases. The Δ_{ZPE} values of our present MEPs depend on: (i) the $H - -C$ vibrations at the TS geometries and (ii) the intramolecular vibrational frequencies within the remaining chain of atoms in the reactants. Since we found that the TS has a linear geometry for $x=1$, but it has increasingly more bent structures for x increasing from 3, to 5, to 7 (see Table 6 and 7 below), then the Δ_{ZPE} is the largest for the HCN member of the series while it becomes increasingly smaller for increasingly larger members of the present series. We report in detail in Tables 6 and 7 all the geometric parameters for the TS structures we have found for our VTST calculations. We should note here that the calculations for $x=1$ and $x=3$ had been carried out already in our earlier work on the present mechanism (Satta et al. 2015), where we employed a smaller basis set expansion for the RPES calculations and carried out the VTST calculations over a less dense grid of points. The present, improved, results remain however within less than 5% of the earlier ones and exhibit exactly the same temperature dependence.

HCN					
T	HH	HC			
10-340	1.721	1.055			
345-475	1.712	1.059			
480-500	1.702	1.062			

<i>HC₃N</i>					
T	HH	HC ₁	HHC ₁	HC ₁ C ₂	C ₁ C ₂ C ₃
10-255	1.713	1.030	158.12	166.31	179.04
260-350	1.702	1.034	158.38	166.00	179.01
355-440	1.692	1.037	158.64	165.69	178.98
445-500	1.681	1.041	158.88	165.37	178.95

Table 6: Computed structures of the TS over a broad range of temperature for the smaller members of the present cyanopolyne chains. Distances in Å, angle in degrees

<i>HC₅N</i>						
T	HH	HC ₁	HHC ₁	HC ₁ C ₂	C ₁ C ₂ C ₃	C ₂ C ₃ C ₄
10-70	1.537	1.056	151.65	156.27	177.22	178.90
75-130	1.524	1.060	152.10	155.74	177.17	178.90
135-190	1.510	1.064	152.53	155.19	177.12	178.90
195-240	1.497	1.067	152.95	154.64	177.07	178.91
245-295	1.483	1.071	153.36	154.09	177.03	178.91
300-350	1.470	1.075	153.75	153.53	176.99	178.91
355-410	1.456	1.079	154.12	152.97	176.95	178.91
415-480	1.442	1.082	154.49	152.41	176.91	178.91
485-500	1.429	1.086	154.84	151.84	176.88	178.91
<i>HC₇N</i>						
T	HH	HC ₁	HHC ₁	HC ₁ C ₂	C ₁ C ₂ C ₃	C ₂ C ₃ C ₄
10-35	1.476	1.062	148.39	153.34	176.52	178.64
40-75	1.462	1.066	148.96	152.69	176.46	178.64
80-115	1.447	1.070	149.51	151.04	176.40	178.65
120-165	1.433	1.074	150.04	151.40	176.35	178.65
170-210	1.418	1.077	150.55	150.76	176.30	178.65
215-270	1.404	1.081	151.03	150.12	176.26	178.66
275-315	1.389	1.085	151.50	149.47	176.22	178.66
320-365	1.375	1.089	151.95	148.84	176.19	178.66
370-420	1.361	1.092	152.37	148.21	176.17	178.67
425-465	1.347	1.096	152.79	147.58	176.14	178.67
470-500	1.333	1.100	153.19	146.96	176.13	178.67

Table 7: Computed structures of the TS over a broad range of temperature for the larger members of the present cyanopolyne chains. Distances in Å, angle in degrees

The data of these Tables show, from the top to the bottom panels, the $x=1$ to $x=7$ cases. The first two columns report distances of the atoms in the complex: the $H^- - H$ and $H - C_1$, while the next columns give angles along the bent structures of the longer members of the series. Only the $H^- - HCN$ reaction shows a linear TS structure.

Since, within the RRKM approach which we have used in the present modeling, the structure of the TS is crucially linked to the expression for the resulting rate coefficient via eq.s (5) and (6), it is interesting to note the following from a perusal of the data reported in the above Tables:

- (i) The structures of the TSs change little over a very broad range of temperatures, indicating that the variational determination of the TS is correctly obtained: along an exothermic, barrierless path the structure of the final complex should change little from its minimum structure;
- (ii) as the length of the chain increases we see more marked departures from linearity along what we have defined as the "translational" coordinates which are active along the MEP and which involve the X-C-H-H bonds, while the C-atoms further away seem to maintain a nearly linear structure. It means that only the nearest triple bond is affected by the polarization changes during the ET process, while those further away along the chain remain largely unchanged, as expected;
- (iii) The modification of that triple bond, on the occurrence of excess charge initial transfer, which reaches its final, main localization at the terminal N atom of the product anion, also affects the Δ_{ZPE} energy gaps discussed before, a feature which is crucial for the low-T behaviour of the rate coefficients (see eq.s 6): it follows then that the Δ_{ZPE} value increases again from $x=3$ to $x=5$ and $x=7$. This feature will be further discussed below when analysing the low-temperature behaviour of the present rates.

We have further fitted all the computed rates following the standard formula suggested earlier for such systems, see: Gianturco et al. (2016); Satta et al. (2015); Prasad and Huntress (1980) and we therefore report the actual fitting parameters in Table 8 for the higher-T range (upper panel) and the low-T range (lower panel). The actual fitting formula is also reported at the bottom of that Table.

The data for the x=1 member of the series will be discussed later on comparison with the HNC isomeric variant.

T (K)	n	α (cm ³ /s)	β	γ (K)
100-500	1	9.0368e-10	1.7361	284.429
	3	2.3052e-9	1.7589e-1	153.699
	5	2.7539e-9	-3.7352e-2	188.310
	7	3.1121e-9	-3.9163e-1	391.083
10-100	1	1.8152e-9	6.4397e-1	479.034
	3	2.4787e-9	4.9065e-2	173.248
	5	2.7820e-9	-4.9593e-2	190.971
	7	2.8484e-9	-2.4470e-1	367.335
$K(T) = \alpha \left(\frac{T}{300}\right)^\beta e^{-\frac{\gamma}{T}}$				

Table 8: Fitting parameters for the rate coefficients computed in the present work, given for the high-T range (upper panel) and the low-T range (lower panel). The actual fitting formula is given at the bottom of the Table.

The temperature behaviour of the computed rates is reported for all present systems by the two panels of Figure 5

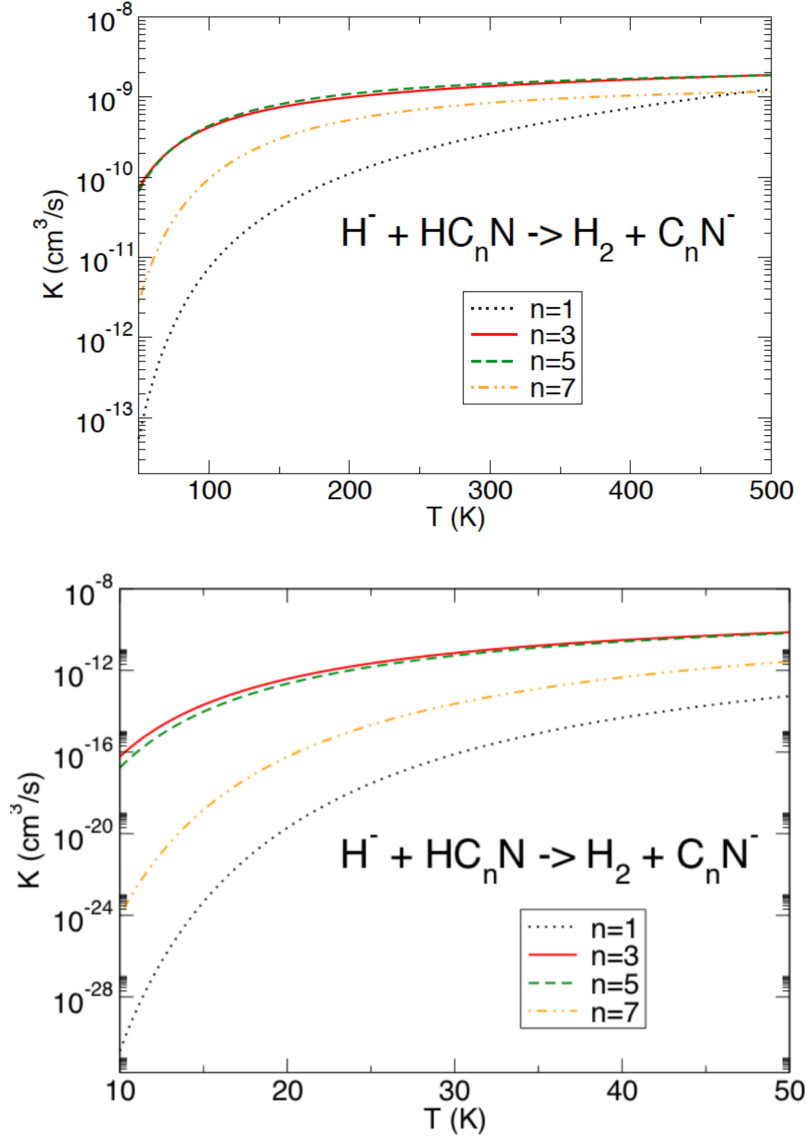


Fig. 5.— Computed temperature dependence of the reaction rates of the present study from CN^- to C_7N^- for the odd values of the x index. The lower panel reports the low-T behaviour, while the upper panel gives the higher-T behaviour of the rates of formation.

The following comments could be made by observing the rate behaviour in that figure:

- (i) as expected, the formation of CN^- remains the least efficient chemical process in reaction with H^- . All other members of the series exhibit larger reaction rates at

all temperatures. As discussed earlier, this feature has to do with the instability of the anion of the molecular reaction partner and therefore with the importance of initiating the ET step only at large bond distances for the H–CN fragment of the reacting cyanopolyynes, where the final hydrogen molecule has not yet been formed. At low temperature that step may not occur while at the higher temperature its increased occurrence is still limited by the fewer degrees of freedom of the PF of its transition complex;

- (ii) The largest rates are seen to occur for the formation of C_3N^- and, close to it in size, by the formation of C_5N^- . These are the two species exhibiting the largest rates of formation from the present calculations. Since both systems were shown to have TS complexes not far from the more efficient linear structures, it stands to reason that both molecular anions are formed with larger rates with respect to those of the $x=1$ system, where the reduced number of degrees of freedom involved in its PFs limits the size of the corresponding rates;
- (iii) The largest member of the series, the C_7N^- shows a smaller rate of formation at all T, smaller than the $x=3$ and 5 members but still larger than the $x=1$ member. This difference has to do with the fact, already discussed earlier, that the TS variationally optimized structures are now far from the linear configurations and therefore the bending of the longer chain attached to the active coordinates reduces the numerator in (5), which in turn lowers the value of the associated reaction rate. It is further worth noting here that, with the exclusion for the moment of the $x=1$ member, the $x=3$ and 5 anions are seen in our calculations to be associated with largest rates of reaction. They are two members of the present series of molecules for which the anions have been repeatedly detected in the ISM, while C_7N^- larger member, so far, has not yet been detected by observational studies (e.g. see: ref Millar et al. (2017));

(iv) One should also note that the Langevin rates listed in the KIDA database of Wakelam and et. al. (2012) for CN^- are about $3.8 \cdot 10^{-9} \text{ cm}^3 \text{ mol}^{-1} \text{ s}^{-1}$ and independent of temperature. They are obviously always overestimating all present rates and at all temperatures.

Another interesting set of comparison between the values of the rates of formation, at a four selected temperatures indicative of different regions of the ISM are reported in Table 9 for the four members of the cyanopolyynes series of this work.

n	10 K	30 K	50 K	100 K
1	2.29(-31)	7.85(-17)	5.53(-14)	7.40(-12)
3	5.96(-17)	7.10(-12)	7.34(-11)	4.19(-10)
5	1.71(-17)	5.29(-12)	6.67(-11)	4.38(-10)
7	8.58(-25)	2.26(-14)	2.75(-12)	9.57(-11)

Table 9: Computed rate values, at four different temperatures, for the present series of cyanopolyynes (units of $\text{cm}^3 \text{ mol}^{-1} \text{ s}^{-1}$)

One sees that at the lowest shown temperature of 10 K the formation of CN^- and C_7N^- are really negligible, while the formation of C_3N^- and C_5N^- is still small but many orders of magnitude larger. The effects are more marked for the region between 30 and 100 K, indicatively corresponding to the averaged temperatures of Dark Molecular Clouds and CSE environments, see: Millar et al. (2017). In these intervals we see that the rates of formation become much larger for all four systems, albeit still being largest for C_3N^- and C_5N^- . Such data indicate that the possibility of forming all anions by chemical routes becomes significant for the latter molecules and in clear competition with REA processes which have been shown as having much smaller rates of formation associated with them. One should also be reminded that for temperatures around 50 K the chemical rates of

formation of the $x=1$ member of the present series are already orders of magnitude larger than its calculated REA rates around 100 K : Khamesian et al. (2016). It therefore follows that even for the smallest member of the present series of anions the chemical paths reported here is much more significant than the REA mechanism for explaining the formation of its anion .

Another interesting comparison between some of our data is shown in the panels of Figure 6, where the rates of formation of CN^- are shown for both the isomer partners of H^- : HCN and HNC.

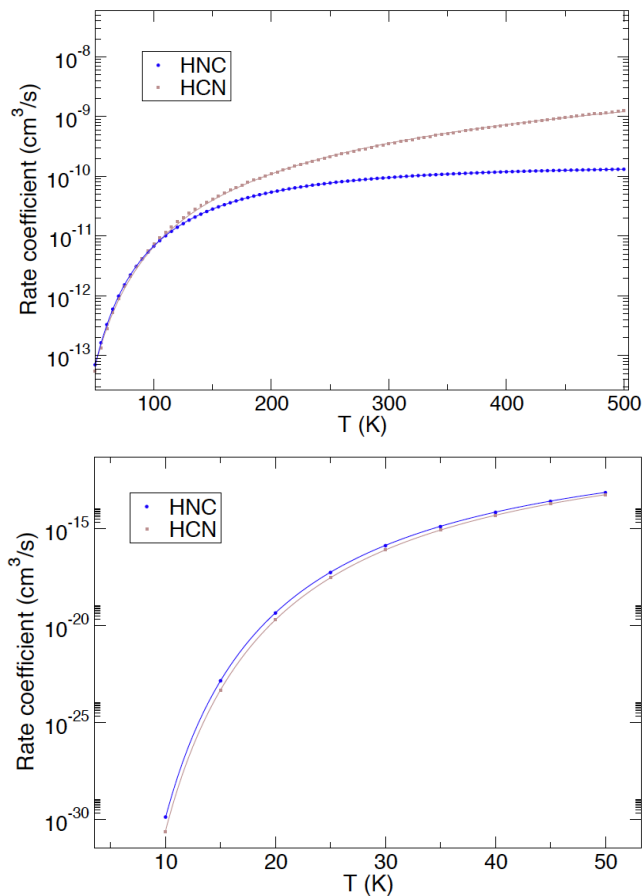


Fig. 6.— Computed formation rates of CN^- from both isomeric forms of the initial reagent: HCN and HNC. See main text for further details. Lower panel: low-T range; upper panel: high-T range

It is interesting to note that both reagents, as expected, behave very similarly as a function of temperature. The low-T formation rates are very close to each other, although the CN^- formation rate from HNC remains always slightly larger. As the temperature

moves above 150 K we see that the differences in size increase and the trend is inverted. We see in the upper panel of fig. 6 that the HNC reagent yields formation rates which are increasingly smaller, reaching nearly one order of magnitude smaller around 500 K. On the whole, however, the rates of formation at 200 K and above remain of the order of 10^{-10} $\text{cm}^3 \text{mol}^{-1} \text{s}^{-1}$, i.e. substantially larger than the corresponding rates of REA formation by electron attachment Herbst and Osamura (2009); Kawaguchi et al. (1995); Khamesian et al. (2016). All reaction rates, however, remain smaller than the Langevin formation rates usually employed in astrochemical databases and which are, as mentioned earlier, of the order of 10^{-9} $\text{cm}^3 \text{mol}^{-1} \text{s}^{-1}$ as given by Wakelam and et. al. (2012).

We summarize in Table 10 the fitting parameters for the two isomeric partners of the smallest member of the present series of cyanoderivatives, both leading to the formation of CN^- .

	HNC		HCN	
T(K)	10-50	50-500	10-50	50-500
$\alpha(\text{cm}^3/\text{s})$	$4.9394 \cdot 10^{-10}$	$5.2509 \cdot 10^{-10}$	$6.9512 \cdot 10^{-10}$	$1.1986 \cdot 10^{-9}$
β	-0.6029	-0.7082	-0.3966	1.4335
$\gamma(K)$	495.3	511.6	507.5	362.1

Table 10: Computed fitting parameters for the T-dependence of the formation rates of CN^- from HNC (left) and HCN (right). The formula is the same as that of Tables 6 and 7. All rates in units of $\text{cm}^3 \text{mol}^{-1} \text{s}^{-1}$.

It is also interesting to comment on the possible reasons for the difference in the temperature dependence of the two rates. We already know that the HC bond is less strong than the HN bond in its isomeric variant, as shown by our data discussed in Section II. We have already discussed before that, at low-T, the present chemical rates are controlled by

the differences in ZPE values between the two TS (linear) for both molecules. Since the one for HCN is larger than for HNC, then the low-T formation rates given by our VTS theory slightly favour the formation from HCN than that from HNC. As the temperature increases, however, the contribution from the CN frequencies in HCN vs HNC are higher in the former with respect to the latter. Furthermore, the opposite occurs for the HC frequency in the TS with respect to the HN frequency: it is about 3311 cm^{-1} in the former and 3643 cm^{-1} in the latter. Thus, as the temperature increases the stronger HN bond within the TS complex slows down the rate increase for HNC vs those for HCN. On the whole, however, both molecules can contribute with similar rates to CN^- formation, thereby making its probability of occurrence even larger than via the REA route (about $10^{-17}\text{ cm}^3\text{ mol}^{-1}\text{ s}^{-1}$ around 100 K: Herbst and Osamura (2009); Khamesian et al. (2016))

5. Present Conclusions

In the present work we have analysed in detail the chemical formation of C_xN^- anionic species from a reaction with H^- of the corresponding cyanopolyynes species: HC_xN , with x from 1 to 7. The aim has been to evaluate, for temperatures of significance under ISM conditions, the relative probabilities of forming the anions and to show that this specific chemical route is likely to be more significant than the more popular electron attachment processes followed by radiative emission which has been considered for a long time as the chief source of those anions, i.e. the REA formation mechanism already discussed many times in the literature Herbst and Osamura (2009); Mackay et al. (1977); Carelli et al. (2014, 2013); Khamesian et al. (2016).

We have carried out structural calculations for the reagents with $x=1, 3, 5, 7$ and further employed accurate ab initio findings to generate the RPES along the collinear path. We have further calculated the nonlinear MEP to product formation. The behaviour of

all the above structural quantities along the series of cyanopolyynes has been discussed in detail in sections II and III.

In section IV we have employed the computed MEP to obtain the anion formation rates of reaction using the VTS theory and examining the effects of nonlinear TS for the longer chains of the series. We thus found that while CN^- is formed via a linear MEP to final RRKM TS that in turns decays into products, the longer chains with $x=3, 5$ and 7 show an increasing importance of non linear TS structures for the formation of the complexes, a feature that finally produces a strongly bent transition complex for the $x=7$ member of the series, and corresponding rates of formation which are lower than those of the two preceeding, smaller terms of the same series.

The calculations of the reaction rates also show a distinct behaviour as a function of temperature: (i) a very rapid increase of several orders of magnitude when going from a few K to about 100 K, and (ii) a smoother increase with temperature when T increases up to 500-1000 K. This behaviour was shown here to be linked to the importance of the ZPE differences between reactants and their TS structures . We found in fact them to be smallest for the C_3N^- formation reaction, so that the latter rates show the largest values in the low-T regimes.

All reactions were found to be strongly exothermic, without a barrier from reactants to products and forming a TS complex along the MEP. It is along that path that the reactants undergo H_2 formation in its lowest vibrational state, following an ET process that begins to take place when forming an initial complex with a highly stretched $H - H$ reagent and finally evolves to the anionic C_xN^- . product The computed rate values reported by Table 9 show that in going from 10 K to 100 K they change differently for each member of the series : the least reactive HCN changes nearly twenty orders of magnitude, while the more efficient formations of C_3N^- and C_5N^- vary by about seven orders of magnitude: the

changes with temperature therefore turn out to be very dramatic, for reasons explained in the previous Section.

In the range of temperatures likely to be present in CSE environments, where those anions have been detected (e.g. see the Review by Millar et al. (2017)) we therefore see that the present chemical process for C_3N^- is several orders of magnitude larger than the REA rate of formation Mackay et al. (1977); Khamesian et al. (2016).

Furthermore, we also see that the size of the Langevin rates of anion formation, usually employed in modelling studies: Wakelam and et. al. (2012), are invariably larger than any of our computed rates. It indicates the low reliability of using such estimates for the present ionic reactions.

Another interesting result from the present calculations is the analysis of the rates of formation for the HCN/HNC isomers. Their relative abundances in the ISM have been discovered to be very different from the one on earth, thus suggesting that both species could contribute equally to the production of CN^- anions. In fact, our calculations for both species, presented in Figure 6, indicate their rates to exhibit some differences as a function of temperature, but to be essentially of the same order of magnitude around 100-200 K. Given the fact that the REA path of formation was found to be several orders of magnitude smaller over the same range of temperature Khamesian et al. (2016), our findings suggest again that the present chemical route to CN^- formation is a more efficient mechanism for forming that anion in the CSE environments or dark molecular clouds.

The present calculations further indicate that the $x=7$ case produces RRKM rates of formation which are smaller than those of the shorter chains with $x=3$ and 5, this being more so in the lower-T range below 50 K. The specific structural reason provided by our calculations indicate that the TS complex along the MEP for this reaction favours strongly bent structures which therefore increase the importance of bending vibrations within the

PF of the complex. This results into a reduction of the rate values obtained within the VTST model.

Such finding is in line with the fact that, thus far, the C_7N^- anionic molecule has not been observed although HC_7N has been observed: Millar et al. (2017). On the other hand, both C_3N^- and C_5N^- have been detected by Gupta et al. (2007); Herbst (1981).

The following conclusions could therefore be drawn from the results of the present calculations:

- (i) The chemical paths to anionic derivatives from initially neutral cyanopolyynes in reaction with H^- are shown to be more effective than the REA paths (whenever available) at the ISM temperature of interest;
- (ii) The C_3N^- and C_5N^- formation exhibit the largest chemical rates in the range of 50 K to 100 K and therefore the present reactions are shown to be very effective mechanisms for their formation;
- (iii) The formation of CN^- can occur via two different reagents, HCN and HNC, which were shown to have very similar rates. Albeit being the smallest found by our calculations, their combined occurrence can be markedly larger than the existing REA rates indicated in the current literature Khamesian et al. (2016), thereby making this chemical reaction an important path to their formation;
- (iv) the C_7N^- formation rates turn out to be smaller than the preceding shorter members of the series, thus suggesting this chemical "inefficiency" as a possible cause for the lack of its observational detection as discussed in Millar et al. (2017).

The present chemical study therefore confirms from ab initio calculations that the analysis of ion-molecule reactions involving H^- should be experimentally attempted with

cyanopolyynes to search for chemical routes to the formation of anionic (C,N)-containing linear chains as those observed already in different ISM environments Millar et al. (2017).

Acknowledgements

F.A.G. and R.W. thank the Austrian Science Fund (FWF) for supporting the present research through the Project P27047-N20.

REFERENCES

- I. Baccarelli, F. Sebastianelli, B. Nestmann, and F. A. Gianturco. *EPJD*, 67:93, 2013.
- P Botschwina and R Oswald. *J. Chem. Phys.*, 129:044305, 2008.
- S. Brunken, H. Gupta, C. A. Gottlieb, M. C. Mc Carthy, and P. Thaddeus. *ApJL*, 664:L43, 2007.
- F Carelli, M. Satta, T. Grassi, and F. A. Gianturco. *Ap. J.*, 774:97, 2013.
- F Carelli, F. A. Gianturco, R. Wester, and Satta M. *Chem. Phys.*, 141:054302, 2014.
- J. Cernicharo, M. Guelin, M. Agundez, K. Kawaguchi, M. C. Mc Carthy, and P. Thaddeus. *Astron. Astrophys.*, 467:L37, 2007.
- R. A. Dalgarno. *Ap. J.*, 1973.
- N. Douguet, S. Fonseca dos Santos, M. Rault, O. Dulieu, A. E. Orel, and V. Kokoouline. *Phys. Rev. A*, 88:052710, 2013.
- A. Fernandez-Ramos, J. A. Miller, S. J. Klippenstein, and D. G. Truhlar. *ChRv*, 106:4518, 2006.
- R. C. Fortenberry and D. T. Crawford. *J. Chem. Phys.*, 134:154304, 2011.
- Y. Gao and P. M. Solomon. *ApJ Supl. Ser.*, 152:63, 2004.
- F. A. Gianturco, M. Satta, M. Mendolicchio, F. Palazzetti, A. Piserchia, V. Barone, and R. Wester. *Astrophys. J.*, 830:2, 2016.
- D. Graninger, K. Oberg, C. Qi, and J. Kostner. *ApJ Lett.*, 807:L15, 2015.
- H. Gupta, F. Brunken, S. Tainassia, C. A. Gottlieb, M. C. Mc Carthy, and P. Thaddeus. *Astrophys. J. Lett.*, 655:L57, 2007.
- E. Herbst. *Nature*, 289:656, 1981.
- E. Herbst and Y. Osamura. *ApJ*, 679:1670, 2009.

- E. Herbst and D. E. Woon. *ApJ*, 489:109, 1997.
- M. R. Hogerheijde, D. J. Jansen, and E. F. van Dishoeck. *A+A*, 294:792, 1995.
- M. jin, J. E. Lee, and K. T. Kim. *ApJ Supl. Ser.*, 219:2, 2015.
- K. Kawaguchi, Y. Kasai, S. Ishikawa, and N. Kaifu. *PASJ*, 47:853, 1995.
- M Khamesian, N. Douguet, S. Fonseca dos Santos, M. Rault, O. Dulieu, W.J. Brigg, , and V. Kokoouline. *Phys. Rev. Lett.*, 117:123001, 2016.
- R. Kolos, M. Gronowski, and P Botschwina. *J. Chem. Phys.*, 128:154305, 2008.
- D. D. Lis, D. Backelee-Morvan, J. Boissier, J. Crovisier, N. Biver, and S. B. Charnley. *ApJ*, 675:931, 2008.
- H. Listz and R. Lucas. *A+A*, 370:576, 2001.
- G. I. Mackay, K. Tanaka, and D. K. Bohme. *IJMIP*, 24:125, 1977.
- M. C. Mc Carthy, C. A. Gottlieb, H. Gupta, and P. Thaddeus. *Astrophys. J. Lett.*, 652:L141, 2006.
- T. J. Millar, C. Walsh, and T. A. Field. *Chem. Rev.*, 117:1765, 2017.
- P. Mily-Blant, M. Walmsley, G. Pineu-des Forets, and D. Flower. *A+A*, 512:A41, 2010.
- R. Moreno, E. Lelouch, L. M. Lara, and et al. *A+A*, 536:L12, 2011.
- Y. Morisawa, H. Hoshina, Y. Kato, Z. Simizu, S. Kuma, N. Sogoshi, M. Fushitani, S. Watanabe, Y. Miyamoto, T. Momose, Y. Kasai, and K. Kawaguchi. *PASJ*, 57:325, 2005.
- S. S. Prasad and T. J. Jr. Huntress. *Astrophys. J. Suppl.*, 43:1, 1980.
- A. J. Remijan, J. M. Hollis, F. J. Lovas, M. A. Cordiner, T. J. Millar, A. J. Markwick-Kemper, and P. R. Jewell. *ApJL*, 664:L47, 2007.
- E. Sarrasin, D. Ben Abdallah, M. Wernli, A. A. Faure, J. Cernicharo, and F. Lique. *MNRAS*, page 518, 2010.

P. J. Sarre. *J. Chem. Phys.*, 77:769, 1980.

M. Satta, F. A. Gianturco, F. Carelli, and R. Wester. *ApJ*, 799:228, 2015.

F. Sebastianelli and F. A. Gianturco. *EPJD*, 59:389, 2010.

F. Sebastianelli and F. A. Gianturco. *EPJD*, 66:41, 2012.

R. C. Shiell, X. K. Hy, Q. C. J. Hu, and J. W. Hepburn. *Far. Disc. Chem. Soc.*, 115:331, 2000.

P. Thaddeus, C. A. Gottlieb, H. Gupta, S. Bruenken, M. C. Mc Carthy, M. Agundez, M. Guelin,
and J. Cernicharo. *Astrophys. J.*, 677:1132, 2008.

R Thomson and F. W. Dalby. *Can. J. Phys.*, 46:2815, 1968.

B. E. Turner, L. Pirogov, and Y. C. Minh. *ApJ*, 483:235, 1997.

O. Wakelam and et. al. <http:kida.obs.u-boreaux1.fr>, 2012.

MOLPRO version 2006.1 a package of ab initio programs Werner, J-H et al. <http://www.molpro.net>,
2006.